Synthesis of High-Density Nanocavities inside TiO2-B Nanoribbons and Their Enhanced Electrochemical Lithium Storage Properties

ARTICLE *in* INORGANIC CHEMISTRY · NOVEMBER 2008

Impact Factor: 4.76 · DOI: 10.1021/ic800758d · Source: PubMed

Inorg. Chem. **2008**, *47*, 9870−9873

Synthesis of High-Density Nanocavities inside TiO_2−B Nanoribbons and Their Enhanced Electrochemical Lithium Storage Properties

Quanjun Li,[†] Jingwei Zhang,[‡] Bingbing Liu,*[,†] Ming Li,[‡] Ran Liu,[†] Xianglin Li,[†] Honglei Ma,[†] Shidan Yu,[†] Lin Wang,[†] Yonggang Zou,[†] Zepeng Li,[†] Bo Zou,[†] Tian Cui,[†] and Guangtian Zou[†]

State Key Laboratory of Superhard Materials, Jilin University, Changchun 130012, P. R. China, and Key Laboratory of Special Functional Materials, Henan University, Kaifeng 475004, P. R. China

Received April 28, 2008

Single crystalline TiO_2−B nanoribbons with high-density nanocavities were successfully synthesized via a simple hydrothermal route. The as-prepared TiO_2−B nanoribbons exhibited a large Brunauer, Emmett, and Teller (BET) surface area of about 305 m^2/g because of the high-density nanocavities inside the thin nanoribbons. Electrochemical measurements indicated that the TiO_2−B nanoribbons with dense nanocavities showed discharge specific capacity higher than those of TiO_2−B nanotubes and nanowires. It was found that the dense nanocavities have an important influence on the electrochemical lithium intercalation properties.

Introduction

In recent years, one-dimensional (1D) TiO_2 nanostructures have attracted much attention due to their various applications in photocatalysts, microelectronics, photovoltaic cells, rechargeable lithium ion batteries, and chemical sensors.[1−8] A variety of efficient synthetic strategies for preparation of 1D nanostructures have been developed. The hydrothermal method is a very facile way for preparation of TiO_2 nanomaterials such as nanowires,[4,6,8] nanotubes,[3,5,7] and nanorods.[7,9] As is well-known, there are four common polymorphs of TiO_2: rutile, anatase, brookite, and TiO_2−B. Among these TiO_2 polymorphs, TiO_2−B has a relatively open structure with significant voids and continuous channels compared with the structures of the other TiO_2 polymorphs, which gives excellent lithium storage performance to the TiO_2−B structure.[1,4,5] In addition, the electrochemical properties depend on a wide variety of factors such as particle size, morphology, crystallinity, and so forth.[10] Recently, TiO_2−B nanowires and nanotubes were extensively studied for use as negative electrode materials in lithium batteries; they showed high specific capacity and good cycle stability under high charge and high discharge rates.[4,5,7,11] However, the electrochemical properties of TiO_2−B nanomaterials need to be improved for actual lithium battery application. One possible way to improve the electrochemical lithium storage properties of TiO_2−B nanomaterials is to enhance the porosity and surface area by forming mesopores or nanocavities. This has been an effective method in other electrode nanomaterials because enhancing the porosity makes it possible to introduce new active reactions in the electrode nanomaterials that decrease the path length for Li ion transport and decrease the specific surface current rate, improving stability and specific capacity.[10,12−14] However, there has been no information on TiO_2−B nanomaterials with mesopores or nanocavities in this field until now. Recently, dense nanocavities inside TiO_2 (anatase) nanorods or nan-

* To whom correspondence should be addressed. E-mail: liubb@jlu.edu.cn. Fax: 86-431-85168256.
† Jilin University.
‡ Henan University.

(1) Bavykin, D. V.; Friedrich, J. M.; Walsh, F. C. *Adv. Mater. (Weinhein, Ger.)* **2006**, *18*, 2807.
(2) Mao, Y. B.; Wong, S. S. *J. Am. Chem. Soc.* **2006**, *128*, 8217.
(3) Kuo, H. L.; Kuo, C. Y.; Liu, C. H.; Chao, J. H.; Lin, C. H. *Catal. Lett.* **2007**, *113*, 7.
(4) Armstrong, A. R.; Armstrong, G.; Canales, J.; Bruce, P. G. *Angew. Chem., Int. Ed.* **2004**, *43*, 2286.
(5) Armstrong, G.; Armstrong, A. R.; Canales, J.; Bruce, P. G. *Chem. Commun. (Cambridge, U.K.)* **2005**, 2454.
(6) Wang, G.; Wang, Q.; Lu, W.; Li, J. H. *J. Phys. Chem. B* **2006**, *110*, 22029.
(7) Zhang, H.; Li, G. R.; An, L. P.; Yan, T. P.; Gao, X. P.; Zhu, H. Y. *J. Phys. Chem. C* **2007**, *111*, 6143.
(8) Wei, M. D.; Qi, Z. M.; Ichihara, M.; Honma, I.; Zhou, H. S. *Chem. Phys. Lett.* **2006**, *424*, 316.
(9) Nian, J. N.; Teng, H. *J. Phys. Chem. B* **2006**, *110*, 4193.
(10) Jiang, C. H.; Hosono, E.; Zhou, H. S. *Nano Today* **2006**, *1*, 28.
(11) Armstrong, A. R.; Armstrong, G.; Canales, J.; Garcia, R.; Bruce, P. G. *Adv. Mater. (Weinheim, Ger.)* **2005**, *17*, 862.
(12) Wang, K. X.; Wei, M. D.; Morris, M. A.; Zhou, H. S.; Holmes, J. D. *Adv. Mater. (Weinheim, Ger.)* **2007**, *19*, 3016.
(13) Wen, Z. H.; Wang, Q.; Zhang, Q.; Li, J. H. *Adv. Funct. Mater.* **2007**, *17*, 2772.
(14) Luo, J. Y.; Zhang, J. J.; Xia, Y. Y. *Chem. Mater.* **2006**, *18*, 5618.

10.1021/ic800758d CCC: $40.75
Published on Web 10/07/2008

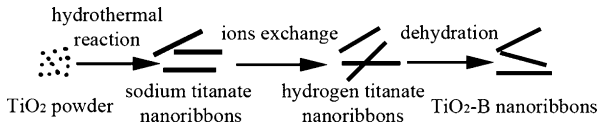

Figure 1. Formation process for TiO_2−B nanoribbons.

oribbons have been prepared by a hydrothermal route.[15] These studies inspired us to synthesize the TiO_2−B nanomaterials with dense nanocavities and to study their electrochemical lithium storage properties. In this article, we design a facile hydrothermal route to prepare TiO_2−B nanoribbons with dense nanocavities that show a high surface area and excellent electrochemical properties.

Experimental Section

Synthesis of TiO_2−B nanowires was performed by the hydrothermal process and post treatments. In a typical synthesis, 0.5 g of TiO_2 (Degussa P25, about 20% rutile and 80% anatase with a particle size of about 20−30 nm) was dispersed in a 14 mL, 10 M NaOH aqueous solution. After stirring for 30 min, the resulting suspension was transferred into a Teflon-lined stainless steel autoclave. The autoclave was maintained at 180 °C for 24 h and then cooled to room temperature naturally. The resulting precipitate was acid washed, which involved stirring the sample in a 0.5 M HCl solution for 8 h. The material was then filtered, washed with distilled water, dried, and finally calcinated at 400 °C for 4 h in air. The sample was characterized using X-ray diffraction (XRD) (Rigaku D/max-RA, step size 0.05, time dwell 0.1 s), transmission electron microscopy (TEM) (200 kV, HITACHI, H-8100IV), and field emission scanning electron microscopy (FESEM) (15 kV, XL 30, ESEM). Specific surface areas were measured by Brunauer−Emmett−Teller (BET) nitrogen adsorption−desorption (Shimadzu, Micromeritics Tristar 3000 Instrument). Electrochemical properties were measured on electrodes prepared by compressing a mixture of active materials, acetylene black, and polyvinylidene fluoride (PVDF) binder in a weight ratio of 80:15:5. Lithium metal was used as the counter and reference electrodes. The electrolyte was $LiPF_6$ (1 M) in a mixture of ethylene carbonate (EC) and dimethyl carbonate (DMC) in a weight ratio of 1:1. The galvanostatic method at the charge−discharge current density of 67 mA/g was used to measure the electrochemical capacity of the electrodes at room temperature using a LAND-CT2001A instrument. The cutoff potentials for charge and discharge were set at 3.0 and 1.0 V versus Li^+/Li, respectively.

Results and Discussion

As shown in Figure 1, the production route for the TiO_2−B nanoribbons involved three processing stages: (1) formation of sodium titanate nanoribbons from the starting TiO_2 powder by a simple hydrothermal reaction, (2) ion exchange to convert the sodium titanate nanoribbons into hydrogen titanate nanoribbons, and (3) dehydration to transform the hydrogen titanate nanoribbons into TiO_2−B nanoribbons with dense nanocavities.

To confirm the crystal structure of the as-prepared sample, we carried out XRD analysis. The XRD pattern of the intermediate product, hydrogen titanate nanoribbons, is shown in pattern a of Figure 2. The structure of the

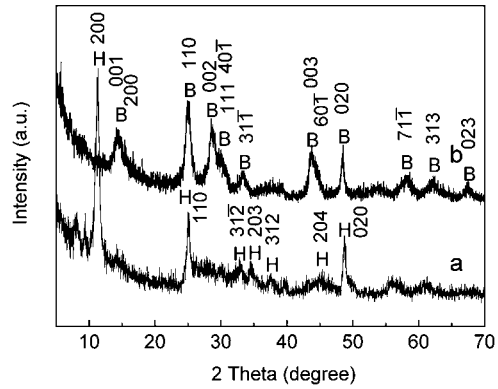

Figure 2. XRD pattern from (a) hydrogen titanate nanoribbons and (b) TiO_2−B nanoribbons: H, hydrogen titanate; B, TiO_2−B.

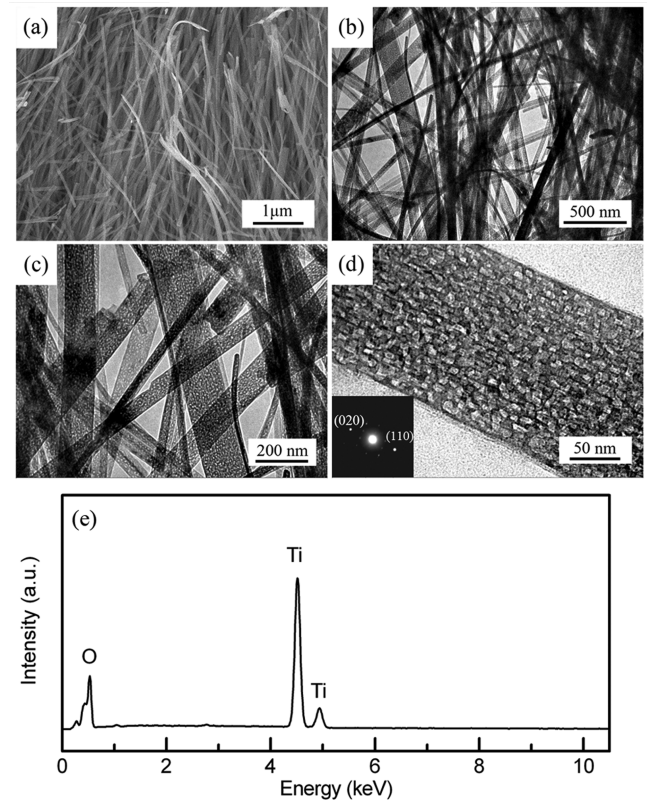

Figure 3. FESEM image (a) and variable magnification TEM images (b, c, and d) of the TiO_2−B nanoribbons. The inset in panel d shows an electron diffraction (ED) pattern. The EDS spectrum of the TiO_2−B nanoribbons is shown in panel e.

intermediate product is similar to that of a layered titanate $H_2Ti_xO_{2x+1}$, which is mainly trititanate ($H_2Ti_3O_7$, JCPDS 41-0192). In a typical hydrothermal synthesis process, hydrogen titanate was obtained by ion exchange through acid washing sodium titanate that was produced by an alkaline hydrothermal treatment as reported.[4,5] In general, at high hydrothermal temperatures above 170 °C, the prepared hydrogen titanate transformed into TiO_2−B rather than anatase TiO_2 after heating to 400 °C in air.[4] In our work, the as-prepared hydrogen titanate was completely converted into TiO_2−B (JCPDS 46-1237) as shown in pattern b of Figure 2.

Figure 3 shows FESEM and TEM images of TiO_2−B nanoribbons. The overall image of TiO_2−B nanoribbons is shown in the FESEM image (Figure 3a) that clearly reveals

(15) Han, W. Q.; Wu, L. J.; Klie, R. F.; Zhu, Y. M. *Adv. Mater. (Weinheim, Ger.)* **2007**, *19*, 2525.

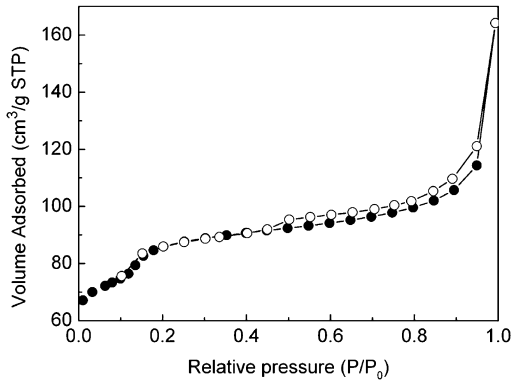

Figure 4. Nitrogen adsorption−desorption isotherms of the TiO_2−B nanoribbons with dense nanocavities: (●) adsorption and (○) desorption.

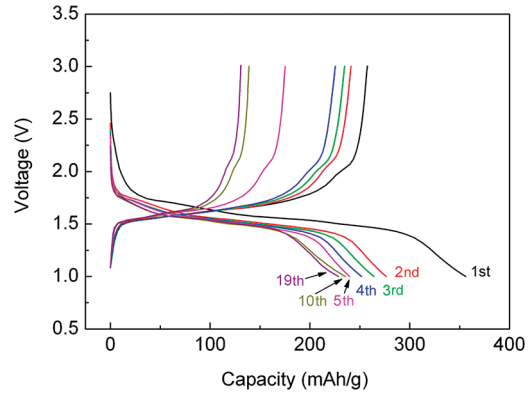

Figure 5. Discharge and charge profiles of TiO_2−B nanoribbons at a constant current density of 67 mAh/g between 1.0 and 3.0 V.

the presence of a large number of uniform nanoribbons several micrometers long. The low-magnification TEM image (Figure 3b) indicates that the width of the nanoribbons varies from 30 to 200 nm. In order to further characterize the nanoribbons, a high-magnification TEM image is shown in Figure 3c. It is obvious that the morphology of the as-synthesized sample is a ribbon-like structure that is very thin (∼20 nm) and has a uniform width (30−200 nm). The dense nanocavities are distributed uniformly on the surfaces of TiO_2−B nanoribbons and can be observed from the light dots, which are nanocavities, on the dark body of TiO_2−B nanoribbons. The TEM image of an individual nanoribbon and its selected area electron diffraction (SAED) pattern are depicted in Figure 3d. It can be seen from Figure 3d that many of the nanocavities observed have a size of ∼10 nm and are distributed densely in the nanoribbons. A typical SAED pattern taken from a single nanoribbon is depicted in the inset in Figure 3d. It reveals that the nanoribbon is a single crystal grown along the [010] direction. Further study confirms that almost all TiO_2−B nanoribbons preferentially grow along the [010] direction. The energy dispersive X-ray spectrum (EDS) of TiO_2−B nanoribbons is shown in Figure 3e. There are no remnant Na^+ ions, which indicates that Na^+ ions were washed thoroughly with a dilute HCl solution.

It has been demonstrated that layered, monoclinic hydrogen titanate can be transformed into the metastable TiO_2−B (monoclinic, space group *C*2/*m*) at 400 °C, and that the anatase phase (tetragonal, space group *I*4/*m*) can be obtained at the higher temperature of 700 °C.[16] In our case, the nanocavities were formed during the dehydration of layered titanate nanoribbons when empty spaces were produced by the evaporation of H_2O. The growth mechanism is also possibly explained by the anti-crystal growth model proposed by Han et al. that is used to explain the forming mechanism of nanocavities in anatase TiO_2 nanorods.[15] These results suggest that the nanocavities inside anatase TiO_2 nanorods derive from further growth of the nanocavities inside TiO_2−B nanoribbons.

The nitrogen adsorption−desorption isotherms at 77 K of TiO_2−B nanoribbons with dense nanocavities are presented in Figure 4. As seen in Figure 4, the adsorption curve gradually increases in the middle-pressure region and exhibits an abrupt increase in the high-pressure region (>0.8 P/P_0), so the adsorption behavior of TiO_2−B nanoribbons can be attributed to the capillary condensation and multilayer adsorption of nitrogen in the mesopores or macropores. This is different from that of the TiO_2−B nanowires reported previously.[6,17] The values of the BET surface area and the total pore volume are 305 m^2/g and 0.204 cm^3/g, respectively. It is obvious that the surface area is much higher than that of the TiO_2−B nanowires[6,17] and close to that of the TiO_2 nanotubes.[7,17] The high surface area can be rationally attributed to the dense nanocavities inside the TiO_2−B nanoribbons.

Figure 5 displays the cyclic discharge−charge curves of an electrode made from TiO_2−B nanoribbons. A high initial discharge capacity of the lithium ions' deintercalation into the as-prepared TiO_2−B nanoribbons is 356 mAh/g. The value corresponds to $x = 1.06$ for Li_xTiO_2−B. It is higher than those of TiO_2−B nanowires (305 mAh/g) and nanotubes (335 mAh/g)[4,5] and close to those of brookite TiO_2 nanoparticles[18] and TiO_2−B@C nanoribbons.[19] The initial discharge capacity of TiO_2−B nanoribbons is less than that of the nanocrystalline rutile TiO_2 (391 mAh/g),[20] which is probably because of the ultrafine size (5 nm) of the nanocrystalline rutile TiO_2. It is suggested that further reducing the size of the nanoribbons might be effective in further improving the discharge capacity of TiO_2−B nanoribbons. The discharge−charge curves exhibit almost monotonic voltage evolution without a constant potential region similar to that of TiO_2−B nanowires and nanotubes reported previously.[7,17,21] The smooth slopes of the voltage curves indicate that lithium intercalation into the TiO_2−B nanoribbons remains a single-phase process after repeated cycles, which means that no two phases are interfacial during the lithium intercalation process. The irreversible capacity

(16) Pavasupree, S.; Suzuki, Y.; Yoshikawa, S.; Kawahata, R. J. *J. Solid State Chem.* **2005**, *178*, 3110.
(17) Wang, Q.; Wen, Z. H.; Li, J. H. *Inorg. Chem.* **2006**, *45*, 6944.
(18) Reddy, M. A.; Pralong, V.; Varadaraju, U. V.; Raveau, B. *Electrochem. Solid-State Lett.* **2008**, *11*, A132.
(19) Li, Q. J.; Zhang, J. W.; Liu, B. B.; Li, M.; Yu, S. D.; Wang, L.; Li, Z. P.; Liu, D. D.; Hou, Y. Y.; Zou, Y. G.; Zou, B.; Cui, T.; Zou, G. T. *Cryst. Growth Des.* **2008**, *8*, 1812.
(20) Reddy, M. A.; Kishore, M. S.; Pralong, V.; Caignaert, V.; Varadaraju, U. V.; Raveau, B. *Electrochem. Commun.* **2006**, *8*, 1299.
(21) Natarajan, C.; Setoguchi, K.; Nogami, G. *Electrochim. Acta* **1998**, *43*, 3371.

of the sample in the first cycle is 80 mAh/g, which is similar to that of TiO_2−B nanowires and obviously larger than that of ordinary nanocrystalline titania.[7,17,21,22] Both the charge and discharge specific capacities tend to decrease with increasing cycling. From the 5th cycle to the 19th cycle, the average capacity loss is less than 0.85 mAh/g, and the high discharge capacity of 229 mAh/g is still retained up to the 19th cycle, which shows good cycle stability.

According to the above results, it is obvious that the high discharge specific capacity and good cycle stability of the sample can be attributed to the large surface area and short transport distances of ions provided by this unique composite structure of dense nanocavities inside thin TiO_2−B nanoribbons. The as-prepared TiO_2−B nanoribbons grow preferentially along the [010] direction with dense nanocavities as shown in Figure 2. The parallel channels along the [010] axis in the TiO_2−B structure provide intercalation sites where lithium ions can be accommodated without any significant distortion of the structure.[23] From Figure 2, we also can observe that the distance between two close nanocavities is about 10−20 nm. This indicates that many channels with lengths of about 10−20 nm are formed along the [010] direction that significantly decrease the diffusion distance of lithium ions and electrons. In addition, a large number of nanocavities inside these thin nanoribbons obviously increases the amount of surface-stored lithium for the high surface area.

Conclusion

Dense nanocavities inside TiO_2−B nanoribbons were synthesized via a facile hydrothermal route. The TiO_2−B nanoribbons grew along the [010] direction with widths of 30−200 nm and lengths of several micrometers. The surface area of the TiO_2−B nanoribbons is large, up to 305 m^2/g, because of the high-density nanocavities inside the nanoribbons. Electrochemical measurements indicate that the TiO_2−B nanoribbons with dense nanocavities show lithium intercalation capacity (356 mAh/g) higher than those of the TiO_2−B nanowires and nanotubes. It was found that the dense nanocavities have an important influence on the electrochemical lithium intercalation properties. This material also may be of interest for a variety of applications such as gas sensors and photocatalysts.

Acknowledgment. This work was supported financially by the National Natural Science Foundation of China (NSFC) (10674053, 20773043, 10574053), the Cultivation Fund of the Key Scientific and Technical Innovation Project of MOE of China (2004-295), the National Basic Research Program of China (2005CB724400, 2001CB711201), the Program for Changjiang Scholars and Innovative Research Team in University (IRT0625), the 2007 Cheung Kong Scholars Program of China, the National Foundation for Fostering Talents of Basic Science (J0730311), and the Project for Scientific and Technical Development of Jilin Province.

IC800758D

(22) Wilhelm, O.; Pratsinis, S. E.; Chambrier, E. D.; Crouzet, M.; Exnar, I. *J. Power Sources* **2004**, *134*, 197.

(23) Zukalova, M.; Kalbac, M.; Kavan, L.; Exnar, I.; Graetzel, M. *Chem. Mater.* **2005**, *17*, 1248.